Title: Myonuclear apoptosis underlies diaphragm atrophy in mechanically ventilated ICU patients.

Authors: Wout J. Claassen[1], Marloes van der Berg[1,3], Rianne. R. Baelde[1], Sylvia Bogaards[1], Luuk Bonis[1], Heleen Hakkeling[1], Arezou Bamyani[1], Gerben J. Schaaf[4], Albertus Beishuizen[5], Chris Dickhoff[2], Reinier A. Boon[1], Leo Heunks[6], Tyler J. Kirby[1,*], Coen A.C. Ottenheijm[1,*]

Affiliations: Amsterdam UMC, location VUmc [1]Department of Physiology,[2]Department of Surgery, Amsterdam, the Netherlands [3]University of Arizona, Department of Cellular and Molecular Medicine, Tucson, AZ, USA [4]Erasmus University Medical Center, Center for Lysosomal and Metabolic Diseases, Rotterdam, the Netherlands, [5]Medisch Spectrum Twente, Intensive care Center, Enschede, the Netherlands. [6]Radboudumc, Department of Intensive Care Medicine, Nijmegen, the Netherlands

*** Correspondence**. Coen A.C. Ottenheijm (c.ottenheijm@amsterdamumc.nl) and Tyler J. Kirby (t.kirby@amsterdamumc.nl)

Author contributions: WJC, CACO and TJK designed the study. WJC and MvB, were responsible for sample collection, WJC, RRB, SB, LB HH, AB, GJS performed experiments in the laboratory. AB, CD, LH were responsible for patient recruitment. WJC, LB, HH and AB were responsible for data collection and management. WJC, LB, HH and AB performed statistical analysis and created figures. WJC drafted the manuscript. CACO, TJK, LH, RAB, and WJC critically revised the manuscript. All authors read and approved the manuscript.

Funding: Supported by NHLBI grant HL-121500 (C.A.C.O.); ZonMW Grant 09120011910004 (C.A.C.O; L.H.)

Running head: Myonuclear apoptosis in the diaphragm of ICU patients

Descriptor number: 4.8 (Mechanical Ventilation: Physiology & Pathophysiology)

Word Count: 44 (must be 3500)

This article has an online data supplement, which is accessible from this issue's table of contents online at www.atsjournals.org

Abstract (236 words)

Rationale. Intensive care unit (ICU) acquired diaphragm weakness is a common consequence of mechanical ventilation (MV). It contributes to difficult weaning, which is associated with increased morbidity and mortality. Diaphragm weakness is caused by a combination of atrophy and dysfunction of myofibers, large syncytial cells that are maintained by a population of myonuclei. Each myonucleus provides gene transcripts to a finite fiber volume, termed the myonuclear domain. Myonuclear loss in myofibers undergoing atrophy is subject to debate. Myonuclear number is a determinant of transcriptional capacity, and therefore critical for muscle regeneration after atrophy.

Objectives. Our objective was to investigate if and how myonuclear number is altered in the diaphragm of mechanically ventilated ICU patients.

Methods. We used a combination of confocal microscopy, transcriptomics, and immunohistochemistry techniques to study myonuclear alterations in diaphragm and quadriceps biopsies from MV ICU patients.

Measurements and Main Results. Patients with established diaphragm atrophy had a reduced myonuclear number and myonuclear domain. Intrinsic apoptotic pathway activation was identified as a potential mechanism underlying myonuclear removal in the diaphragm of mechanically ventilated ICU patients. Total transcription of myofibers decreased with myonuclear loss. Furthermore, muscle stem cell number was reduced in the patients with diaphragm atrophy.

Conclusion. We identified myonuclear loss due to intrinsic apoptotic pathway activation as a mechanism underlying diaphragm atrophy in mechanically ventilated patients. The loss of myonuclei may contribute to difficult weaning due to impaired regrowth of myofibers after atrophy.

Introduction

Intensive care unit (ICU) acquired diaphragm weakness is a common consequence of mechanical ventilation (MV). It contributes to difficult weaning, which is associated with increased morbidity, mortality, and healthcare costs (1). Furthermore, it can lead to physical disability and impairment in intensive care survivors (2). Diaphragm weakness is caused by a combination of atrophy and dysfunction of the remaining contractile material, leading to weakness of muscle cells (i.e. myofibers). In previous years, several mechanisms underlying ICU-acquired diaphragm weakness have been identified (3, 4), including changes in myosin confirmation and increased proteolysis (5-7). Mitochondrial dysfunction and apoptosis were identified to underlie diaphragm atrophy in controlled MV rodents and brain-dead organ donors, but not in MV ICU patients (8, 9).

Myofibers are large syncytial cells that are maintained by a population of post-mitotic myonuclei. Each myonucleus provides gene transcripts to a finite fiber volume, termed the myonuclear domain (10-13). Myonuclear loss in myofibers undergoing atrophy is subject to debate (14-18). In an MV rat model of diaphragm atrophy, myonuclear domain was maintained during atrophy due to an apoptotic-like mechanism causing myonuclear loss (7). In MV rodents, myonuclear apoptosis occurred before the onset of atrophy, suggesting a mechanistic role for apoptosis. In line with such a role, inhibiting myonuclear apoptosis attenuated atrophy (7). The fate of myonuclei in the weak diaphragm of MV ICU patients is unknown. Although models of ICU-acquired diaphragm dysfunction show upregulated apoptosis and myonuclear loss (7, 9) brain-dead organ donors and controlled-ventilated rodents do not adequately reflect the diaphragm pathophysiology in MV ICU patients (8). It is critical to investigate whether myonuclear apoptosis occurs in MV ICU patients as, during weaning, the diaphragm needs to regain mass for which nuclear number and their transcriptional activity are important (19, 20). Furthermore, loss of myonuclei may prolong weaning and lead to longer-term functional impairment after hospital discharge.

Our objective was to investigate whether myonuclear number is altered in the diaphragm of mechanically ventilated ICU patients. Hence, we studied myonuclear number and morphology in myofibers isolated from diaphragm biopsies of mechanically ventilated ICU patients. To study whether changes in myonuclear number occur before the onset of atrophy, we also included an ICU group without atrophy. Furthermore, we performed next-generation RNA-sequencing and immunofluorescence labeling of diaphragm cryosections to identify the underlying pathways. Additionally, we obtained quadriceps biopsies of MV ICU patients to investigate whether our findings were specific to the diaphragm. We found a reduced myonuclear number in tandem with atrophy and identified apoptosis as a mechanism underlying myonuclear removal. Apoptosis of myonuclei was increased before the onset of atrophy in both diaphragm and quadriceps muscle. Some of the results of these studies have been previously reported in the form of an abstract (21).

Methods

For further details on the applied methods, see the online supplement.

Patients, diaphragm biopsies

Diaphragm muscle biopsies were obtained from intensive care unit (ICU) patients receiving invasive mechanical ventilation (*ICU* patients, n = 24) and patients undergoing elective lung surgery for early-stage lung malignancy without critical illness (*Control* patients, n=10). Exclusion criteria were chronic obstructive pulmonary disease (≥ GOLD stage III), congestive heart failure, neuromuscular diseases, chronic metabolic disorders, pulmonary hypertension, chronic use of corticosteroids (> 7.5mg/day for at least 3 months), and more than 10% weight loss within the last 6 months. The exclusion criteria were similar for all experimental groups. Patients' characteristics of the two groups are presented in Tables 1 and tables S1/S2. The biopsy protocol was approved by the institutional review board at Amsterdam UMC (location VUmc), the Netherlands. Patients were recruited in Amsterdam UMC and the Netherlands Cancer Institute-Antoni van Leeuwenhoek Hospital (both in Amsterdam, the Netherlands),

and Medisch Spectrum Twente (Enschede, the Netherlands). Written informed consent was obtained from the patients or their legal representative.

Patients, quadriceps biopsies

Quadriceps biopsies of ICU patients (n=10) were obtained in the context of a separate study that has been filed in the Clinical Trial Register under #NCT03231540 and was approved by the Medical Ethical Committee of VU Medical Center, Amsterdam, the Netherlands. Informed consent was obtained from the patient or a legal representative. Patients ≥18 years that had an expected ventilation duration of ≥72 hours, were expected to tolerate enteral nutrition ≥72 hours, and had a Sequential Organ Failure Assessment (SOFA) score ≥6, were considered eligible for inclusion. Exclusion criteria were contra-indications to enteral nutrition, short bowel syndrome, type C liver cirrhosis or acute liver failure, dependency on renal replacement therapy, requiring another specific enteral nutrition formula for medical reasons, BMI >35 kg/m2, extensive treatment limitations, disseminated malignancy, hematological malignancy, primary neuromuscular pathology, chronic use of corticosteroids for >7 days before ICU admission or contra-indications for muscle biopsy such as the need for continuous systemic anticoagulation, prothrombin time >1.3 or thrombocytes <100.

Single myofiber microscopy

Single myofibers were manually isolated from the biopsies. Myonuclear number, myofiber volume, myonuclear morphology, and RNA-polymerase-II Ser5 fluorescence were determined using immunofluorescence labeling in combination with confocal microscopy.

RNA-sequencing

RNA was extracted using a commercially available kit and sequenced using a NextSeq500 (Illumina).

Immunohistochemistry

Serial cryosections were cut from the biopsies and stained to study myonuclear number, myonuclear domain, markers for apoptosis, and PAX7.

Results

Diaphragm biopsies were collected from 24 mechanically ventilated ICU patients who underwent laparotomy or thoracotomy for a clinical indication. The biopsies were collected from the left anterolateral part of the zone of apposition of the diaphragm. In Table 1 we summarize the clinical parameters. The mechanically ventilated ICU patients were divided into a group with diaphragm atrophy (myofiber cross-sectional area (CSA) < 2000 um^2, mean of 1317 um^2), and a group without atrophy (myofiber CSA>2500 um^2, mean of 3442 um^2) (Fig. S1). The biopsies were compared to the biopsies of 10 patients who underwent elective thoracic surgery for a small, primary pulmonary nodule (controls; mean myofiber CSA of 2343 um^2). The groups were matched for age, body mass index, and sex, and the ICU groups were matched for the duration of mechanical ventilation (Table 1). Due to the limited size of the biopsies, not every biopsy was used in every experiment. Table S1 details which biopsies were used for which experiment.

Decreased myonuclear number in atrophic diaphragm fibers

We determined the myonuclear number within myofibers that were randomly selected and manually isolated from the biopsies. Immunofluorescent staining of myonuclear marker pericentreolar-material-1 (PCM1) (22) revealed that the proportion of myonuclei within the isolated myofibers (n = 3 control and n = 3 ICU) was >98% in both groups (Fig. S2). Fast and slow-twitch fibers were identified by immunoreactivity for fast-twitch myosin heavy chain isoform II and data were segregated according to fiber-type (Fig. 1A-B). As expected, myofiber volume was ~50% smaller in the ICU group with atrophy when compared with the ICU group without atrophy and the control group, and this decrease was similar for both fiber types (Fig. 1C). In the ICU group with atrophy, myonuclear number was reduced by about 35% in both fast and slow myofibers when compared to the ICU group without atrophy and the control group (Fig. 1D). To verify whether our findings in single myofibers were representative for a larger sample, we validated these findings by analyzing the number of myonuclei per myofiber in diaphragm muscle cross-sections with an average size of 498

myofibers per section. Myonuclei were identified using PCM1 labeling in combination with localization within the dystrophin barrier. In muscle cross-sections, average myonuclear counts per fiber were reduced by about 39% in the ICU group with atrophy compared to the control group (Fig. S4), consistent with the results from the isolated myofibers (Fig. 1D). Myonuclear domain size was smaller in the ICU group with atrophy when compared to the control group, but not when compared to the ICU group without atrophy (Fig. 1E). When we examined the relationship between fiber CSA and myonuclear number, we found a similar positive correlation in all three groups (Fig. S5). Myonuclear domain size and fiber CSA showed a similar positive correlation, but the slope of the regression line in the ICU group with atrophy was significantly lower, indicating smaller myonuclear domains for the same CSA. The slope of the regression line of the fibers isolated from the biopsies of ICU patients without atrophy had a significantly steeper relationship between myonuclear domain and cross-sectional area in the ICU group without atrophy. Thus, myonuclear number is reduced in muscle fibers isolated from the atrophic diaphragm of mechanically ventilated ICU patients, and myonuclear domain is smaller, indicating more atrophy than myonuclear loss. Furthermore, these changes were absent in the diaphragm of similar ICU patients without established atrophy. Thus, atrophic diaphragm myofibers have a reduced number of myonuclei.

Changes in myonuclear morphology

In addition to myonuclear number, myonuclear size is known to scale with myofiber size (23). Based on the changes we observed in myonuclear number, we sought to study potential changes in myonuclear morphology by segmenting every 3D-rendered nucleus present within the Z-stacks of the myofibers (Fig. 2A). In ICU patients with atrophy, myonuclear volume was reduced (Fig. 2B), and the cumulative fluorescence intensity of the nuclear lamina (lamin A/C) within each nucleus was increased (Fig. 2C). An increased total fluorescent intensity of the nuclear lamina may indicate increased nuclear wrinkling or increased thickness of the nuclear lamina. To further study this, we determined the wrinkling

index of each nucleus by measuring the standard deviation of the fluorescence intensity within each segmented nucleus in maximum intensity Z-projections of the Z-stacks (Fig. 2D) (24). Nuclear wrinkling was increased in the ICU group with atrophy, when compared to the other groups (Fig. 2E). Mean ellipticity or sphericity, two shape descriptors of sphere-like objects, were not different between the groups (Fig. S6 A-B). Thus, nuclear morphology is affected in the diaphragm ICU patients with or without atrophy. This may be a consequence of reduced strain on myofibers caused by mechanical unloading by the ventilator.

Diminished transcriptional activity of myofibers in the atrophic diaphragm of mechanically ventilated ICU patients

Myonuclear number has been shown to influence myonuclear transcription (25, 26). Thus, we aimed to determine if the changes in myonuclear number and morphology resulted in changes in myonuclear transcription in ICU patients. We hypothesized that diminished transcriptional activity contributes to atrophy in ICU patients. Furthermore, transcriptional activity may scale down with the reduced myonuclear domain size in ICU patients with atrophy, because the cellular volume to regulate is smaller. The transcriptional activity of each nucleus was determined by measuring the fluorescent intensity of phosphorylated Serine 5 on RNA-polymerase-2. This phosphorylation occurs shortly after the initiation of transcription, before the capping of the mRNA (27, 28) (Fig. 3A), and has been shown to strongly correlate with transcriptional activity (29, 30). We measured the intensity of the immunofluorescence of activated RNA-polymerase-2 within each nucleus (Fig. 3B) from ten randomly selected myofibers of 5 patients from the ICU group with atrophy and 5 controls (Table 2). We did not include ICU patients without atrophy in this experiment because we expected no changes in transcriptional activity in the absence of atrophy and myonuclear loss. Total transcriptional activity per fiber was calculated by summation of the fluorescence intensity of RNA-pol-II Ser5 labeling within each nucleus present in the myofiber and was on average almost two-fold lower in the ICU group compared to the control group (Fig. 3C). This can be explained by the lower myonuclear number in ICU myofibers, because the

fluorescence intensity of RNA-Pol-II Ser5 per nucleus did not differ between the groups (Fig. 3D). After normalization to fiber volume, the difference in transcriptional activity per fiber was absent (Fig. 3E). Thus, based on these findings, insufficient transcriptional activity of individual nuclei is unlikely to contribute to atrophy, whereas the reduced myonuclear number in the ICU group with atrophy may reduce total transcriptional activity per myofiber.

Transcriptomics reveals upregulation of apoptotic pathways in the diaphragm

To further investigate the mechanisms underlying atrophy and myonuclear loss, we performed next-generation RNA-sequencing of whole tissue samples cut from the biopsies. Principal component analysis (PCA) revealed clear clustering in the control patients, while the ICU groups showed a more variable clustering pattern, with no distinct clustering between the two ICU groups (with or without atrophy) (Fig. 4A). Thus, we decided to perform our analysis on two groups, a group consisting of both ICU groups (with and without atrophy) and the control group (Table 3). We identified 2977 differentially expressed genes (1741 upregulated in the ICU group and 1236 downregulated (Fig. 4B) between control and ICU patients. A heatmap of the top 50 differentially expressed genes was generated (Fig. 4C). Next, we performed Panther pathway enrichment analysis of significant (FDR < 0.2, dashed line represents *p*-value of 0.05) differentially expressed genes (Fig. 4D). The top upregulated pathways in the ICU group were the p53, apoptosis, and integrin signaling pathways. Thus, in mechanically ventilated ICU patients, the p53 and apoptosis pathways are upregulated (Fig. 4E), (Fig. S7), providing a potential mechanism underlying atrophy, weakness, and myonuclear loss.

Caspase-3-mediated apoptosis of myonuclei

To investigate whether apoptotic processes can explain the reduced myonuclear number in ICU patients with atrophy, we performed analyses on muscle cross-sections to allow for the identification of different cell types that may be undergoing apoptosis. Importantly, we used multiple markers to distinguish myonuclei from non-myonuclei (e.g. PCM1 and

dystrophin/laminin immunolabeling), as it has been suggested that much of the apoptosis that occurs during muscle atrophy can be attributed to the non-myonuclear cell pool (17) (22). Tables 4 and 5 show the characteristics of the patients included in these experiments. Using terminal deoxynucleotidyl transferase dUTP nick end labeling (TUNEL) of double-stranded DNA breaks (Fig. 5A), we determined the percentage of myonuclei undergoing apoptosis. Representative images of TUNEL labeling of a DNase-I treated diaphragm section (positive control) are shown in Fig. S8. The TUNEL-index (number of TUNEL-positive myonuclei divided by the total number of myonuclei) in the ICU group without atrophy was almost double that of the control group (Fig. 5B). TUNEL-index was higher in the ICU-group with atrophy, but this difference was not statistically significant. There was no difference in TUNEL-index for other cell types (Fig. S9A). Furthermore, we used antibody for cleaved Caspase-3 (i.e. activated) to investigate the role of caspase-3 mediated nuclear apoptosis (Fig. 5C) (31). The mean activated caspase-3 index (number of cleaved caspase-3-positive myonuclei divided by the total number of myonuclei) was also almost two-fold higher in both ICU groups (Fig. 5D). There was no difference in caspase-3-index for other cell types (Fig. S9B). Next, to investigate whether our findings are specific to the diaphragm, we obtained quadriceps muscle biopsies *n = 10*) and compared them to healthy controls (*n = 5*). *Tables 6 and 7* show the clinical characteristics of this group compared to the diaphragm group. Note that the duration of mechanical ventilation and disease severity are similar in both groups. The percentage of myonuclei undergoing apoptosis was determined using the same activated caspase-3 immunofluorescence protocol as was used for the diaphragm biopsies (Fig. S10A). In the ICU group, the activated caspase-3 index of both myonuclei and other cell types was almost double that of the control group (Fig. S10B, C). The mean myofiber CSA and number of myonuclei per myofiber were similar in the ICU and control groups (Fig. S10 D, E), indicating that in the quadriceps of MV ICU patients, caspase-3 activation occurs before the onset of atrophy and myonuclear loss, and consistent with our results in the diaphragm where active caspase-3 was increased even in the ICU group without atrophy

(Fig. 5E). The activated caspase-3 index was more than two-fold lower in the quadriceps (median of 2.9%) compared to the diaphragm (median of 8.7% and 5.7%) (Fig. S11).

Thus, both our transcriptomic and immunofluorescence data support a mechanism where caspase-3-mediated apoptosis underlies myonuclear loss during ICU-acquired diaphragm weakness. This may have profound implications for weaning and recovery after ICU and hospital discharge, as in the diaphragm, this process appears to commence before the onset of atrophy or changes in myonuclear number in limb muscle.

Decreased muscle stem cell number in the diaphragm of ICU patients

After muscles undergo atrophy that is accompanied by loss of myonuclei (Fig. 1) and transcriptional capacity (Fig. 3), myonuclear number could be restored by the contribution of satellite cells, the resident stem cells present adjacent to myofibers that contribute to myofiber homeostasis (32). Interestingly, muscle stem cell activity is particularly high in the diaphragm (33, 34). Thus, we aimed to investigate whether the muscle stem cell population in the atrophic diaphragm is affected, as this could further impair muscle recovery after atrophy. First, in our RNA-seq data set, we found a lower relative expression of *PAX7*, a transcript uniformly expressed in muscle stem cells (35), (Figure S7B) in both ICU groups compared to the control group. Next, we performed immunofluorescent labeling for *PAX7* to determine the number of muscle stem cells in diaphragm cross-sections (Fig. 6A). Patient characteristics of the groups used in these experiments are shown in table 8. In ICU patients with atrophy, satellite cell content was reduced when normalized for either the number of fibers present within the section (Fig. 6B) or when normalized for total section area (Fig. 6C). In conclusion, satellite cell content is reduced in the atrophic diaphragm of mechanically ventilated patients, potentially impeding the restoration of myonuclear number during recovery.

Discussion

This is the first study to reveal myonuclear loss during diaphragm atrophy in mechanically ventilated ICU patients. We show that myonuclear loss drives a reduction in transcriptional activity within myofibers. Myonuclear loss likely contributes to atrophy because an increased number of apoptotic myonuclei was observed in ICU patients not (yet) exhibiting atrophy. Using next-generation RNA sequencing, we identified intrinsic apoptotic pathway activation as an underlying mechanism. We confirmed this by using two assays to detect apoptotic cells, combined with immunofluorescence identification of bonafide myonuclei using both the myonuclear marker PCM1 and dystrophin to demarcate the myofiber border. Reduced myonuclear number in atrophic myofibers implies that recovery of strength requires the provision of new myonuclei from satellite cells, instead of solely increasing protein synthesis to recover lost contractile material (Fig. 7) (36). Having lost a significant number of myonuclei may put patients at a disadvantage during weaning, because muscle growth and recovery is associated with myonuclear number (19, 20). Additionally, we found a reduced number of satellite cells in the atrophic diaphragm of ICU patients, possibly leading to further impairment of recovery after atrophy. Discovery of this underlying mechanism may pave the way for new treatments.

Myonuclear apoptosis in the diaphragm

In the patients included in this study, TUNEL index was higher in the ICU group with atrophy, but this difference was not statistically significant. This unexpected result may be explained by the fact that the ICU group with atrophy had already lost a significant number of myonuclei, and biopsies may have been procured later in the disease course. The activated caspase-3 index was significantly higher in both ICU groups compared to the control group. This discrepancy between both indices may be due to caspase-3 activation occurring earlier than the formation DNA breaks during the apoptotic process (37), possibly resulting in a longer time window for detection. The fate of myonuclei in muscles undergoing atrophy is subject to debate (15-17). The changes in myonuclear number and domain during atrophy

likely depend on the type of atrophic stimulus (10, 38). Our observation that mechanical ventilation may cause caspase-3-mediated apoptosis of myonuclei is in accordance with the findings of a study investigating diaphragm atrophy in mechanically ventilated rats (6 and 12 h) (7). The authors reported no changes in myonuclear domain size, indicating atrophy that was proportional to myonuclear loss. In our study, the myonuclear domain was significantly smaller in the ICU group with established atrophy compared to controls, implying more or faster atrophy than myonuclear loss. There are several potential explanations for this discrepancy. First, we used 3D rendering of Z-stacks of confocal images to measure myonuclear domain volume within single myofibers, a more sensitive method compared to the myonuclear domain surface area (2D) measurements done on muscle cross-sections in the rodent study (14). Furthermore, the patients in this study had a median ventilation duration of more than 60 hours, much longer than the 12 hours in the rodent study. In larger clinical studies, duration of ventilation was associated with the degree of diaphragm atrophy. The longer time on mechanical ventilation in our study may explain the reduction in myonuclear domain size, with atrophy outpacing myonuclear loss (39). Finally, unlike critically ill patients, the mechanically ventilated rodents were previously healthy. Common conditions in the ICU such as systemic inflammation and increased metabolic demand may independently cause muscle wasting, further accelerating atrophy (40). In quadriceps muscle biopsies of ICU patients, we showed increased caspase-3 mediated apoptosis, albeit at a lower level than in the diaphragm, indicating caspase-3 activation before the onset of muscle wasting, independent of MV. In the quadriceps of MV ICU patients, atrophy has been shown to occur at a later time point (7 days) after ICU admission (41). The pathophysiology of diaphragm atrophy has also been evaluated in mechanically ventilated braindead organ donors (5). Oxidative stress and mitochondrial dysfunction were shown to activate the intrinsic pathway leading to caspase-3 activation and apoptosis (9). In diaphragm biopsies of mechanically ventilated ICU patients, a redox imbalance was proposed to underlie diaphragm atrophy in the absence of mitochondrial dysfunction or oxidative stress. This discrepancy is likely due to the difference in clinical features between brain-dead organ

donors and mechanically ventilated ICU patients (8). We report the first transcriptomic profile of the diaphragm of mechanically ventilated ICU patients. Our main findings are the upregulation of 20 genes associated with the p53 pathway, as well as the upregulation of 16 genes associated with apoptosis. Because p53 is subject to redox regulation, a redox imbalance may activate the pathway (42). The p53 pathway was upregulated in various animal models of muscle atrophy. In mouse soleus muscle after 48 of hind limb suspension, the p53 pathway was upregulated and the apoptotic index was increased (43). In a recent study in mechanically ventilated rabbits, the p53 pathway was upregulated and was hypothesized to contribute to VIDD via increased senescence (44). Interestingly, the p53 and apoptosis pathways were not upregulated in a transcriptomics study of the atrophic diaphragm of controlled mechanically ventilated rats (45). This demonstrates the disparity between animal models and clinical reality, further underlining the need to study pathophysiology in samples from patients. Finally, 19 genes associated with the integrin pathway were upregulated in the diaphragm of ICU patients. This pathway is associated with the transmission of forces from the extracellular matrix to actin, and has been shown to be upregulated after eccentric (lengthening) contractions (46). Eccentric contractions of the diaphragm have been hypothesized to occur during ineffective efforts, premature cycling or reverse triggering, a ventilator asynchrony that has been shown to contribute to diaphragm dysfunction and myofiber injury in pigs with high respiratory effort (47, 48). Therefore, our data support a role for eccentric contractions in the pathophysiology of ICU-acquired diaphragm dysfunction.

Decreased number of satellite cells in the mechanically ventilated diaphragm

Our results show that the number of *PAX7* expressing cells is reduced in the diaphragm of mechanically ventilated ICU patients. This may be a direct effect of increased apoptosis, but we did not perform a separate experiment to quantify apoptotic satellite cells. Only a small fraction of cells in our cross-sections expressed *PAX7* (0.05-0.1%) Therefore, is technically challenging to capture apoptotic satellite cells, especially because of diaphragm biopsy size

limitations. Whether satellite cells are required for muscle regeneration depends on the type of atrophy, and on whether myonuclei are lost during atrophy (32, 49). Nevertheless, lineage tracing studies demonstrated that satellite cell activity is particularly high in the diaphragm under non-diseased conditions (33, 34). In addition, there are likely interstitial stem cells that can contribute to myofibers that do not express *PAX7* (50-53). Future studies should determine the prevalence of non-satellite cell myogenic progenitors in the diaphragm of humans, and whether these cells are a significant source of myonuclei during diaphragm muscle homeostasis. The role of satellite cells during recovery after diaphragm atrophy warrants further investigation. Satellite cell content was reduced in the quadriceps of mechanically ventilated patients with sustained atrophy after 6 months, suggesting a crucial role for satellite cells during muscle regeneration (54).

Disturbed sarcomeric integrity is accepted as one of the mechanisms contributing to ICU-acquired diaphragm weakness (6). In non-diseased conditions, muscle can repair its sarcomeres, as damage occurs during both exercise and normal use. After sarcomeres are damaged, nuclear movement to a site of injury is required for repair (55, 56). During this process, myonuclei migrate toward damaged muscle sections to supply mRNA for sarcomeric proteins, allowing the reassembly of the contractile machinery (55). This mechanism may be disturbed in ICU-acquired diaphragm weakness because sarcomeric damage and reduced myonuclear number are present simultaneously (6).

Clinical implications

The identification of intrinsic apoptotic pathway activation as a mechanism underlying diaphragm atrophy in MV ICU patients may open therapeutic venues to prevent diaphragm weakness and weaning failure. The intrinsic apoptotic pathway plays a central role in a large number of pathologies (57). Therefore, many inhibitors targeting the different components of this pathway have been developed (58). Especially caspase-3 inhibition has been investigated extensively (7, 59). Unfortunately, none have progressed beyond pre-clinical studies, probably due to functions of caspase-3 outside of the intrinsic apoptotic pathway

(59). However, there are other strategies to limit apoptosis, such as limiting ROS production or inhibiting other constituents of the intrinsic apoptotic pathway, such as BAX or BAK (58, 60). More preclinical research is necessary to further explore these targets. Even though our data does not suggest that apoptotic pathway activation is limited to the diaphragm, we only observed myonuclear loss in the presence of myofiber atrophy, suggesting an important role for preventive strategies such as diaphragm protective mechanical ventilation or diaphragm pacing (61, 62).

Limitations

The population of ICU patients included in this is highly heterogeneous, with varying medical histories, reasons for admission, duration of mechanical ventilation, and underlying pathophysiology. Therefore, it is not feasible to search for clinical predictors associated with myonuclear apoptosis or myofiber atrophy with our sample size. Nevertheless, this diverse group of patients does adequately reflect the general ICU population. Due to the invasiveness of taking diaphragm biopsies, the controls in this study are patients undergoing surgery for a pulmonary nodule. We cannot rule out an effect of the clinical status of the controls on the diaphragm, even though the in-and-exclusion criteria should minimize this. Furthermore, due to biopsy size limitations, not all experiments were performed on all biopsies.

Conclusion

In mechanically ventilated patients in the ICU, myonuclear apoptosis is a pathomechanism underlying ICU-acquired diaphragm atrophy. Using a combination of advanced microscopy and molecular biology techniques, we identified p53 activation as the underlying pathway in ICU patients. Myonuclear loss in combination with a reduction of the satellite cell population may compromise recovery of the diaphragm, thereby contributing to weaning failure.

Funding: Supported by NHLBI grant HL-121500 (C.A.C.O.); ZonMW Grant 09120011910004 (C.A.C.O; L.H.)

References

1. Dres M, Demoule A. Diaphragm dysfunction during weaning from mechanical ventilation: an underestimated phenomenon with clinical implications. Crit Care. 2018;22(1):73.
2. Esteban A, Anzueto A, Frutos F, Alia I, Brochard L, Stewart TE, et al. Characteristics and outcomes in adult patients receiving mechanical ventilation: a 28-day international study. JAMA. 2002;287(3):345-55.
3. Penuelas O, Keough E, Lopez-Rodriguez L, Carriedo D, Goncalves G, Barreiro E, Lorente JA. Ventilator-induced diaphragm dysfunction: translational mechanisms lead to therapeutical alternatives in the critically ill. Intensive Care Med Exp. 2019;7(Suppl 1):48.
4. Zhang J, Feng J, Jia J, Wang X, Zhou J, Liu L. Research progress on the pathogenesis and treatment of ventilator-induced diaphragm dysfunction. Heliyon. 2023;9(11):e22317.
5. Levine S, Nguyen T, Taylor N, Friscia ME, Budak MT, Rothenberg P, et al. Rapid disuse atrophy of diaphragm fibers in mechanically ventilated humans. N Engl J Med. 2008;358(13):1327-35.
6. Hooijman PE, Beishuizen A, Witt CC, de Waard MC, Girbes AR, Spoelstra-de Man AM, et al. Diaphragm muscle fiber weakness and ubiquitin-proteasome activation in critically ill patients. Am J Respir Crit Care Med. 2015;191(10):1126-38.
7. McClung JM, Kavazis AN, DeRuisseau KC, Falk DJ, Deering MA, Lee Y, et al. Caspase-3 regulation of diaphragm myonuclear domain during mechanical ventilation-induced atrophy. Am J Respir Crit Care Med. 2007;175(2):150-9.
8. van den Berg M, Hooijman PE, Beishuizen A, de Waard MC, Paul MA, Hartemink KJ, et al. Diaphragm Atrophy and Weakness in the Absence of Mitochondrial Dysfunction in the Critically Ill. Am J Respir Crit Care Med. 2017;196(12):1544-58.
9. Tang H, Lee M, Budak MT, Pietras N, Hittinger S, Vu M, et al. Intrinsic apoptosis in mechanically ventilated human diaphragm: linkage to a novel Fos/FoxO1/Stat3-Bim axis. FASEB J. 2011;25(9):2921-36.
10. Verheul AJ, Mantilla CB, Zhan WZ, Bernal M, Dekhuijzen PN, Sieck GC. Influence of corticosteroids on myonuclear domain size in the rat diaphragm muscle. J Appl Physiol (1985). 2004;97(5):1715-22.
11. Hansson KA, Eftestol E, Bruusgaard JC, Juvkam I, Cramer AW, Malthe-Sorenssen A, et al. Myonuclear content regulates cell size with similar scaling properties in mice and humans. Nat Commun. 2020;11(1):6288.
12. Bagley JR, Denes LT, McCarthy JJ, Wang ET, Murach KA. The myonuclear domain in adult skeletal muscle fibres: past, present and future. J Physiol. 2023;601(4):723-41.
13. Hansson KA, Eftestol E. Scaling of nuclear numbers and their spatial arrangement in skeletal muscle cell size regulation. Mol Biol Cell. 2023;34(8).
14. Snijders T, Aussieker T, Holwerda A, Parise G, van Loon LJC, Verdijk LB. The concept of skeletal muscle memory: Evidence from animal and human studies. Acta Physiol (Oxf). 2020;229(3):e13465.
15. Kirby TJ, Dupont-Versteegden EE. Cross Talk rebuttal: Kirby and Dupont-Versteegden. J Physiol. 2022;600(9):2085-6.
16. Kirby TJ, Dupont-Versteegden EE. Cross Talk proposal: Myonuclei are lost with ageing and atrophy. J Physiol. 2022;600(9):2077-80.
17. Schwartz LM, Gundersen K. Cross Talk opposing view: Myonuclei do not undergo apoptosis during skeletal muscle atrophy. J Physiol. 2022;600(9):2081-4.
18. Eftestol E, Psilander N, Cumming KT, Juvkam I, Ekblom M, Sunding K, et al. Muscle memory: are myonuclei ever lost? J Appl Physiol (1985). 2020;128(2):456-7.
19. Petrella JK, Kim JS, Mayhew DL, Cross JM, Bamman MM. Potent myofiber hypertrophy during resistance training in humans is associated with satellite cell-mediated myonuclear addition: a cluster analysis. J Appl Physiol (1985). 2008;104(6):1736-42.

20. Blocquiaux S, Gorski T, Van Roie E, Ramaekers M, Van Thienen R, Nielens H, et al. The effect of resistance training, detraining and retraining on muscle strength and power, myofibre size, satellite cells and myonuclei in older men. Exp Gerontol. 2020;133:110860.
21. Claassen WJ, Kirby TJ, Heunks LM, Ottenheijm CA. ICU-acquired diaphragm weakness: the role of the myonucleus. Intensive Care Med Exp. 2022(10 (suppl 2)):257-8.
22. Winje IM, Bengtsen M, Eftestol E, Juvkam I, Bruusgaard JC, Gundersen K. Specific labelling of myonuclei by an antibody against pericentriolar material 1 on skeletal muscle tissue sections. Acta Physiol (Oxf). 2018;223(4):e13034.
23. Windner SE, Manhart A, Brown A, Mogilner A, Baylies MK. Nuclear Scaling Is Coordinated among Individual Nuclei in Multinucleated Muscle Fibers. Dev Cell. 2019;49(1):48-62 e3.
24. Cosgrove BD, Loebel C, Driscoll TP, Tsinman TK, Dai EN, Heo SJ, et al. Nuclear envelope wrinkling predicts mesenchymal progenitor cell mechano-response in 2D and 3D microenvironments. Biomaterials. 2021;270:120662.
25. Cramer AAW, Prasad V, Eftestol E, Song T, Hansson KA, Dugdale HF, et al. Nuclear numbers in syncytial muscle fibers promote size but limit the development of larger myonuclear domains. Nat Commun. 2020;11(1):6287.
26. Kirby TJ, Patel RM, McClintock TS, Dupont-Versteegden EE, Peterson CA, McCarthy JJ. Myonuclear transcription is responsive to mechanical load and DNA content but uncoupled from cell size during hypertrophy. Mol Biol Cell. 2016;27(5):788-98.
27. Komarnitsky P, Cho EJ, Buratowski S. Different phosphorylated forms of RNA polymerase II and associated mRNA processing factors during transcription. Genes Dev. 2000;14(19):2452-60.
28. Cho EJ, Takagi T, Moore CR, Buratowski S. mRNA capping enzyme is recruited to the transcription complex by phosphorylation of the RNA polymerase II carboxy-terminal domain. Genes Dev. 1997;11(24):3319-26.
29. Jeronimo C, Bataille AR, Robert F. The writers, readers, and functions of the RNA polymerase II C-terminal domain code. Chem Rev. 2013;113(11):8491-522.
30. Bataille AR, Jeronimo C, Jacques PE, Laramee L, Fortin ME, Forest A, et al. A universal RNA polymerase II CTD cycle is orchestrated by complex interplays between kinase, phosphatase, and isomerase enzymes along genes. Mol Cell. 2012;45(2):158-70.
31. Fry CS, Porter C, Sidossis LS, Nieten C, Reidy PT, Hundeshagen G, et al. Satellite cell activation and apoptosis in skeletal muscle from severely burned children. J Physiol. 2016;594(18):5223-36.
32. Sambasivan R, Yao R, Kissenpfennig A, Van Wittenberghe L, Paldi A, Gayraud-Morel B, et al. Pax7-expressing satellite cells are indispensable for adult skeletal muscle regeneration. Development. 2011;138(17):3647-56.
33. Pawlikowski B, Pulliam C, Betta ND, Kardon G, Olwin BB. Pervasive satellite cell contribution to uninjured adult muscle fibers. Skelet Muscle. 2015;5:42.
34. Keefe AC, Lawson JA, Flygare SD, Fox ZD, Colasanto MP, Mathew SJ, et al. Muscle stem cells contribute to myofibres in sedentary adult mice. Nat Commun. 2015;6:7087.
35. von Maltzahn J, Jones AE, Parks RJ, Rudnicki MA. Pax7 is critical for the normal function of satellite cells in adult skeletal muscle. Proc Natl Acad Sci U S A. 2013;110(41):16474-9.
36. Bruusgaard JC, Gundersen K. In vivo time-lapse microscopy reveals no loss of murine myonuclei during weeks of muscle atrophy. J Clin Invest. 2008;118(4):1450-7.
37. Earnshaw WC, Martins LM, Kaufmann SH. Mammalian caspases: structure, activation, substrates, and functions during apoptosis. Annu Rev Biochem. 1999;68:383-424.
38. Aravamudan B, Mantilla CB, Zhan WZ, Sieck GC. Denervation effects on myonuclear domain size of rat diaphragm fibers. J Appl Physiol (1985). 2006;100(5):1617-22.
39. Schepens T, Verbrugghe W, Dams K, Corthouts B, Parizel PM, Jorens PG. The course of diaphragm atrophy in ventilated patients assessed with ultrasound: a longitudinal cohort study. Crit Care. 2015;19:422.
40. Petrof BJ. Diaphragm Weakness in the Critically Ill: Basic Mechanisms Reveal Therapeutic Opportunities. Chest. 2018;154(6):1395-403.

41. Puthucheary ZA, Rawal J, McPhail M, Connolly B, Ratnayake G, Chan P, et al. Acute skeletal muscle wasting in critical illness. JAMA. 2013;310(15):1591-600.
42. Eriksson SE, Ceder S, Bykov VJN, Wiman KG. p53 as a hub in cellular redox regulation and therapeutic target in cancer. J Mol Cell Biol. 2019;11(4):330-41.
43. Ferreira R, Neuparth MJ, Vitorino R, Appell HJ, Amado F, Duarte JA. Evidences of apoptosis during the early phases of soleus muscle atrophy in hindlimb suspended mice. Physiol Res. 2008;57(4):601-11.
44. Shen W, Jiang Y, Xu Y, Qian X, Jia J, Ding Y, et al. Cellular senescence contributes to mechanical ventilation-induced diaphragm dysfunction by upregulating p53 signalling pathways. BMC Pulm Med. 2023;23(1):509.
45. Liu R, Li G, Ma H, Zhou X, Wang P, Zhao Y. Transcriptome profiling of the diaphragm in a controlled mechanical ventilation model reveals key genes involved in ventilator-induced diaphragmatic dysfunction. BMC Genomics. 2021;22(1):472.
46. Boppart MD, Mahmassani ZS. Integrin signaling: linking mechanical stimulation to skeletal muscle hypertrophy. Am J Physiol Cell Physiol. 2019;317(4):C629-C41.
47. Garcia-Valdes P, Fernandez T, Jalil Y, Penailillo L, Damiani LF. Eccentric Contractions of the Diaphragm During Mechanical Ventilation. Respir Care. 2023;68(12):1757-62.
48. Damiani LF, Engelberts D, Bastia L, Osada K, Katira BH, Otulakowski G, et al. Impact of Reverse Triggering Dyssynchrony during Lung-Protective Ventilation on Diaphragm Function: An Experimental Model. Am J Respir Crit Care Med. 2022;205(6):663-73.
49. Jackson JR, Mula J, Kirby TJ, Fry CS, Lee JD, Ubele MF, et al. Satellite cell depletion does not inhibit adult skeletal muscle regrowth following unloading-induced atrophy. Am J Physiol Cell Physiol. 2012;303(8):C854-61.
50. Gaulton N, Wakelin G, Young LV, Wotherspoon S, Kamal M, Parise G, et al. Twist2-expressing cells reside in human skeletal muscle and are responsive to aging and resistance exercise training. FASEB J. 2022;36(12):e22642.
51. Flynn CGK, Ginkel PRV, Hubert KA, Guo Q, Hrycaj SM, McDermott AE, et al. Hox11-expressing interstitial cells contribute to adult skeletal muscle at homeostasis. Development. 2023;150(4).
52. Murach KA, Confides AL, Ho A, Jackson JR, Ghazala LS, Peterson CA, Dupont-Versteegden EE. Depletion of Pax7+ satellite cells does not affect diaphragm adaptations to running in young or aged mice. J Physiol. 2017;595(19):6299-311.
53. Liu N, Garry GA, Li S, Bezprozvannaya S, Sanchez-Ortiz E, Chen B, et al. A Twist2-dependent progenitor cell contributes to adult skeletal muscle. Nat Cell Biol. 2017;19(3):202-13.
54. Dos Santos C, Hussain SN, Mathur S, Picard M, Herridge M, Correa J, et al. Mechanisms of Chronic Muscle Wasting and Dysfunction after an Intensive Care Unit Stay. A Pilot Study. Am J Respir Crit Care Med. 2016;194(7):821-30.
55. Roman W, Pinheiro H, Pimentel MR, Segales J, Oliveira LM, Garcia-Dominguez E, et al. Muscle repair after physiological damage relies on nuclear migration for cellular reconstruction. Science. 2021;374(6565):355-9.
56. Roman W, Munoz-Canoves P. Muscle is a stage, and cells and factors are merely players. Trends Cell Biol. 2022;32(10):835-40.
57. Vitale I, Pietrocola F, Guilbaud E, Aaronson SA, Abrams JM, Adam D, et al. Apoptotic cell death in disease-Current understanding of the NCCD 2023. Cell Death Differ. 2023;30(5):1097-154.
58. Li K, van Delft MF, Dewson G. Too much death can kill you: inhibiting intrinsic apoptosis to treat disease. EMBO J. 2021;40(14):e107341.
59. Dhani S, Zhao Y, Zhivotovsky B. A long way to go: caspase inhibitors in clinical use. Cell Death Dis. 2021;12(10):949.
60. Powers SK, Hudson MB, Nelson WB, Talbert EE, Min K, Szeto HH, et al. Mitochondria-targeted antioxidants protect against mechanical ventilation-induced diaphragm weakness. Crit Care Med. 2011;39(7):1749-59.

61. Panelli A, Verfuss MA, Dres M, Brochard L, Schaller SJ. Phrenic nerve stimulation to prevent diaphragmatic dysfunction and ventilator-induced lung injury. Intensive Care Med Exp. 2023;11(1):94.
62. Goligher EC, Jonkman AH, Dianti J, Vaporidi K, Beitler JR, Patel BK, et al. Clinical strategies for implementing lung and diaphragm-protective ventilation: avoiding insufficient and excessive effort. Intensive Care Med. 2020;46(12):2314-26.

Figure legends

Figure 1. Reduced amount of myonuclei in atrophic diaphragm fibers of critically ill patients.

A: Representative images of single muscle fibers from control (left) and ICU (right) patients. Myofibers are immunofluorescently labeled for lamin A/C (red) and myosin heavy chain (green) Scale bar = 60 µm **B:** Representative images of 3D rendered single muscle fibers, with segmentation in 3D. Scale bar= 60 µm. **C:** Quantification of myofiber volume, calculated as volume per mm fiber was normalized to a sarcomere length of 2.5 µm. Every grey dot represents the value of a single muscle fiber and the colored symbols represent the mean values of a single patient. Slow-twitch fibers: ICU A+ N = 14, n = 84; N = 10, n = 50; CTRL N = 10, n = 48. Fast-twitch fibers: ICU A+ N = 14, n = 56; ICU A− N = 10, n = 48; CTRL N = 10, n = 46. **D:** Quantification of myonuclear number. Every grey dot represents the value of a single muscle fiber and the colored symbols represent the mean values of a single patient. Slow-twitch fibers: ICU A N = 14, n = 84; ICU A− N = 10, n = 50; CTRL N = 10, n = 48. Fast-twitch fibers: ICU A+ N = 14, n = 56; ICU A− N = 10, n = 48; CTRL N = 10, n = 46. **E:** Quantification of myonuclear domain size. Every grey dot represents the value of a single muscle fiber and the colored symbols represent the mean values of a single patient. Significance levels were calculated using linear mixed models with the patients as the random factor. Black bars indicate the median of the whole group. Slow-twitch fibers: ICU A N = 14, n = 84; ICU A− N = 10, n = 50; CTRL N = 10, n = 48. Fast-twitch fibers: ICU A+ N = 14, n = 56; ICU A− N = 10, n = 48; CTRL N = 10, n = 46. ICU A+ = ICU group with atrophy; ICU A− = ICU group without atrophy; CTRL = Control group. * denotes $p < 0.05$; ** denotes $p < 0.01$. N = number of patients, n = number of analyzed myofibers

Figure 2. Altered myonuclear morphology in diaphragm myofibers of ICU patients. **A:** Representative images of unsegmented (left) and segmented (right) 3D-rendered myonuclei within mounted single muscle fibers that were immunofluorescently labeled for lamin A/C. Note the difference in ellipticity and sphericity between the top and the bottom myonucleus. Scale bar = 5 µm. **B:** Representative images of maximum intensity Z-projections of Z-stacks of myonuclei. Note the difference between the nuclei with a smooth nuclear lamina (left) and a wrinkled nuclear lamina (right). Scale bar = 5 µm. **C:** Quantification of myonuclear volume. Each grey dot represents the value of a single nucleus. Each colored symbol represents the mean value of a single patient. The black bar represents the mean value within the groups of patients. Significance level was calculated using linear mixed models with the patients as the random factor. CTRL N = 10 patients, n = 6270 nuclei; ICU A+ N = 14 patients; n = 5463 nuclei; ICU A− N = *10* patients; n = 6330 nuclei. **D:** Quantification of lamin A/C fluorescence intensity within each nucleus. Each grey dot represents the value of a single nucleus. Each colored symbol represents the mean value of a single patient. The black bar represents the mean value within the groups of patients. Significance level was calculated using linear mixed models with the patients as the random factor. CTRL N = 10 patients, n = 6270 nuclei; ICU A+ N = 14 patients, n = 5463; ICU A− N = 10 patients, n = 6330 nuclei. **E:** Quantification of the wrinkling index for each nucleus. Wrinkling index was calculated as the standard deviation of the fluorescence intensity within the segmented nucleus. Each grey dot represents the value of a single nucleus. Each colored symbol represents the mean value of a single patient. The black bar represents the mean value within the groups of patients. Significance level was calculated using linear mixed models with the patients as the random factor. CTRL N =10 patients, n = 1983 nuclei; ICU A+ N = 14 patients, n = 2601 nuclei; ICU A− N = 10 patients, n = 2442 nuclei. ICU A+ = ICU group with atrophy; ICU A− = ICU group without atrophy; CTRL = Control group. * denotes $p < 0.05$; ** denotes $p < 0.01$;

Figure 3. Transcriptional activity of myonuclei in the diaphragm

A: Schematic of RNA-polymerase-II with phosphorylation at Serine 5 with antibody binding to phosphorylated Serine. This phosphorylation occurs when RNA-Pol-II starts transcribing DNA into RNA. **B:** Representative images of RNA-Pol-II-Ser5 (magenta), lamin A/C (yellow), and phalloidin (green) labeling of a single Z-plane of a mounted single muscle fiber. Z-stacks were used to create 3D renders of fiber segments and total RNA-Pol-II Ser5 fluorescence intensity was measured within each myonucleus, using lamin A/C to segment all nuclei in 3D. Scale bar = 20 µm. **C:** Total RNA-Pol-II-Ser5 fluorescence intensity was calculated as the sum of the total RNA-Pol-II-Ser5 fluorescence intensity within each nucleus present within three Z-stacks generated from a single myofiber. CTRL *N =5* patients, *n* = 48 myofibers; ICU A+ *N* = 5 patients, *n* = 48 myofibers. Each grey symbol represents the value of a single myofiber. Each colored symbol represents the mean value of a single patient. **D:** Total RNA-Pol-II-Ser5 fluorescence intensity per segmented nucleus. CTRL *N* =5 patients, *n* = 2817 nuclei; ICU A+ *N =5* patients, *n* = 2235 nuclei. Each grey symbol represents the value of a single nucleus. Each colored symbol represents the mean value of a single patient. **E.** Total RNA-Pol-II-Ser5 fluorescence intensity per myofiber volume was calculated as the sum of the total RNA-Pol-II-Ser5 fluorescence intensity within each nucleus present within the myofiber divided by the myofiber volume. CTRL *N =5* patients, *n* = 48 myofibers; ICU A+ *N* = *5* patients, *n* = 48 myofibers. Each grey symbol represents the value of a single myofiber. Each colored symbol represents the mean value of a single patient. The black bar represents the mean value within the groups of patients. Significance level was calculated using linear mixed models with the patients as the random factor. ICU A+ = ICU group with atrophy; CTRL = Control group; * denotes $p < 0.05$; ** denotes $p < 0.01$

Figure 4. RNA sequencing of the diaphragm of mechanically ventilated ICU patients.

A: Principal component analysis of sequencing results. Note the clustering of the samples within the CTRL group while this clustering is absent in both ICU groups. This may be due to heterogeneity of patient characteristics within both ICU groups. Based on these results, we

decided to pool all ICU patients in a single group for further analysis. CTRL *N* = 8; ICU *N* = 17. **B:** Volcano plot and **C:** top 50 DEG heatmap. Top50 most significantly differentially expressed DEGs for each contrast (sorted by smallest adjusted *p*-value). 1714 genes were significantly upregulated and 1236 genes that were significantly downregulated in the ICU group. Genes with a significance level <0.05 and a fold change of >1.5 were deemed differentially expressed. CTRL *N* = 8; ICU *N* = 17. **D:** PANTHER gene set enrichment analysis. Top10 gene sets or pathways enriched for up- or down-regulated genes of one database (dashed line: *p*-value = 0.05). Only shows pathways that are not significant for both directions (up/down) at the same time to identify on/off situations. Significant gene set enrichment is defined by the false discovery rate. CTRL *N* = 8; ICU *N* = 17. **E:** Schematic of the differentially expressed genes that are involved in the intrinsic apoptotic pathway. Genes in green are significantly upregulated and genes in red are significantly downregulated in ICU patients.

Figure 5. Caspase-3 mediated apoptosis as a mechanism underlying myonuclear loss in the atrophic diaphragm of ICU patients.

A: Representative images of diaphragm muscle cross-sections stained with TUNEL assay, PCM1 antibody, Dystrophin antibody, and DAPI. Nuclei with a TUNEL-positive signal were designated as apoptotic myonuclei when they were PCM1 positive and were located within the dystrophin barrier. Note the difference in PCM1 positivity of the TUNEL+ non-myonucleus (left white arrow) and myonucleus (right white arrow). Scale bar top row is 50 µm, scale bar bottom row is 20 µm. **B:** Quantification of TUNEL index, calculated as the percentage of TUNEL-positive myonuclei. Total myonuclear count was determined by counting PCM1-positive nuclei. The grey bar represents the median value within the groups of patients. Each colored symbol represents the value of a single patient. CTRL *N* = 11; ICU A− *N* = 7; ICU A+ *N* = 14. Significance level was calculated using one-way ANOVA. **C:** Representative images of diaphragm muscle cross-sections stained with Cleaved caspase-3 antibody, PCM1 antibody, Laminin antibody and DAPI. Nuclei with a Cleaved Caspase-3 positive signal were

designated as apoptotic myonuclei when they were PCM1 positive and were located within the laminin barrier. Scale bar top row = 50µm, scale bar bottom row = 20 µm. **D:** Quantification of activated caspase-3 index**,** calculated as the percentage of activated caspase-3-positive myonuclei. Total myonuclear count was determined by counting PCM1-positive nuclei. The grey bar represents the median value within the groups of patients. Each colored symbol represents the value of a single patient. CTRL *N* = 7; ICU A− *N* = 6; ICU A+ *N* = 7 . Significance level was calculated using Kruskal-Wallis test. ICU A+ = ICU group with atrophy, ICU A− = ICU group without atrophy, CTRL = Control group, * = $p<0.05$, ** = $p<0.01$

Figure 6. Decreased abundance of PAX7 positive cells in the atrophic diaphragm

A: Representative images of diaphragm muscle cross-sections stained with PAX7 antibody, Laminin antibody, and DAPI. Nuclei with a PAX7-positive signal were designated as satellite cells. Scale bar = 50 µm in the top row and 10 µm in the bottom row. **B:** Number of PAX7 positive cells present in diaphragm muscle cross sections, normalized for section size. The grey bar represents the median value within the groups of patients. Each colored symbol represents a single patient. CTRL *N* = 6; ICU *N* = 8. Significance level was calculated using Mann-Whitney U test. **C:** Number of PAX7 positive cells present in diaphragm muscle cross sections, normalized for the number of myofibers. The grey bar represents the median value within the groups of patients, brackets represent interquartile ranges. Every colored symbol represents a single patient. CTRL *N* = 6; ICU *N* = 8. Significance level was calculated using Mann-Whitney-U test.

ICU = ICU group with atrophy, CTRL = Control group, * = $p<0.05$, ** = $p<0.01$

Figure 7. Graphical summary

Graphical summary of findings.

Table 1. Clinical characteristics of patients

Characteristic	Control (n = 10)	ICU, atrophy (n =14)	ICU, no atrophy (n=10)	P-value
Age (years) [IQR]	67 [60-72]	65 [55-71]	60 [49-69]	0.600
Male (%)	7 (70)	7(50)	8 (80)	
BMI (Kg/m^2)	28 [24-32]	25 [21-28]	26 [21-28]	0.219
APACHE-3	-	78 [53-149]	75[67-89]	0.875
Ventilation (hours)	1.5 [0.9-2.0]	63 [45-121]	90 [18-223]	<0.001
Myofiber CSA (µm^2)	2469 [1708-2973]	1341 [1007-1667]	3159 [2798-4294]	<0.001
Medical history, n (%)				
Smoking	3 (30)	9 (64)	3 (30)	0.062
COPD ≤ G2	3 (30)	2 (14)	1 (10)	0.482
Other lung disease	2 (20)	1 (7)	0 (0)	0.277
Cardiac	1 (10)	2 (14)	1 (10)	0.930
Arterial vascular disease	2 (20)	11 (79)	2 (20)	0.003
Hypertension	3 (30)	6 (43)	3 (30)	0.742
CKD	1 (10)	2 (14)	0 (0)	0.472
T2DM	0 (0)	0 (0)	2 (20)	0.078
Hypothyroidism	0 (0)	2 (14)	1 (10)	0.471
CID	0 (0)	0 (0)	0 (0)	-
Malignancy lung	7 (70)	0 (0)	1 (10)	<0.001
Malignancy other	2 (20)	0 (0)	6 (60)	0.004
Blood gas Median, [IQR]				
pH (min)		7.13 [7.05-7.32]	7.27 [7.21-7.32]	0.875
pO_2 (min), mmHg		67 [49-74]	58 [47-83]	0.450
pCO_2 (max), mmHg		44 [34-50]	56 [48-67]	0.011
Bicarbonate (min), mmol/l		13 [10-17]	18 [14-21]	0.230
Lactate (max), mmol/l		7.7 [3.2-10.1]	3.7 [1.4-6.0]	0.580
P/F-ratio (min)		135 [107-287]	146 [102-223]	0.196
A-a gradient (max)		190 [101-251]	242 [156-314]	0.027
Medication				
Steroids	-	11 (79)	9 (90)	0.375
Neuromuscular blockers	-	8 (57)	4 (40)	0.309
Vasopressors	-	10 71)	9 (90)	0.198

Data displayed as Median [IQR], p-values calculated with Kruskal-Wallis or chi-squared tests BMI: Body Mass Index, MVhr: duration of mechanical ventilation before biopsy *BMI = Body Mass Index APACHE = Acute Physiology And Chronic Health Evaluation, CSA = Cross-Sectional Area, COPD = Chronic Obstructive Pulmonary Disease, CKD = Chronic Kidney Disease, T2DM = Type 2 Diabetes Mellitus, CID = Chronic Inflamamtroy Disease, P/F-ratio = arterial partial pressure of oxygen (PaO2) divided by the inspired oxygen concentration (FiO2), A-a gradient = alveolar-arterial gradient.*

Table 2. Patient characteristics in transcriptional activity of nuclei experiment

	Control (n=5)	ICU atrophy (n=5)	P-value
Age	64 [61-68]	62 [61-71]	1.0
Male (%)	3 (60)	3 (60)	1.0
BMI	29 [27-31]	25 [20-25]	0.032
APACHE-3	-	57 [53-87]	-
Ventilation (hours)	1.0 [0.6-1.5]	63 [45-84]	0.008
Myofiber CSA (μm^2)	2501 [1975-3129]	1318 [797-17]	0.032

BMI = Body Mass Index APACHE = Acute Physiology And Chronic Health Evaluation, CSA = Cross-Sectional Area

Table 3. Patient characteristics in RNA-sequencing experiment

	Control (n=9)	ICU atrophy (n=9)	ICU no atrophy (n=8)	P-value
Age (years)	64 [51-71]	67 [51-70]	65 [36-82]	0.908
M (%)	7 (78)	3 (33)	5 (63)	0.153
BMI (Kg/m^2)	24 [23-30]	24 [20-28]	27 [24-28]	0.333
APACHE-3	-	100 [62-113]	64 [57-74]	0.163
Ventilation (hours)	1.3 [0.9-2]	57 [42-169]	46 [44-189]	<0.001
Myofiber CSA(μm^2)	3127 [2592-3679]	1706 [1406-1840]	3077 [2242-3805]	<0.001

BMI = Body Mass Index APACHE = Acute Physiology And Chronic Health Evaluation, CSA = Cross-Sectional Area

Table 4. Patient characteristics in TUNEL experiment

	Control (n=8)	ICU atrophy (n=11)	ICU no atrophy (n=8)	P-value
Age (years)	67 [58-73]	67 [58-73]	58 [44-68]	0.359
M (%)	5 (63)	7 (64)	7 (88)	0.364
BMI (Kg/m^2)	27 [24-29]	25 [23-31]	26 [20-28]	0.686
APACHE-3	-	61 [43-129]	74 [67-84]	0.833
Ventilation (hours)	1.5 [0.9-2.0]	102 [61-272]	90 [17-196]	<0.001
Myofiber CSA(μm^2)	2501 [1582-3127]	1191 [897-1449]]	3722 [2969-4473]	<0.001

BMI = Body Mass Index APACHE = Acute Physiology And Chronic Health Evaluation, CSA = Cross-Sectional Area

Table 5. Patient characteristics in Caspase-3 staining experiment

	Control (n=7)	ICU atrophy (n=8)	ICU no atrophy (n=6)	P-value
Age (years)	66 [60-71]	62 [53-70]	59 [38-69]	0.695
M (%)	4 (57)	5 (63)	5 (83)	0.577
BMI (Kg/m^2)	26 [24-28]	24 [21-27]	26 [22-28]	0.478
APACHE-3	-	54 [15-124]	73 [66-75]	0.770
Ventilation (hours)	1.0 [0.9-1.8]	65 [62-173]	42 [17-198]	0.001

Myofiber CSA (μm^2)	2501 [1720-3024]	1192 [952-1420]	3723 [3008-4453]	<0.001

BMI = Body Mass Index APACHE = Acute Physiology And Chronic Health Evaluation, CSA = Cross-Sectional Area

Table 6. Characteristics of individual patients of quadriceps studies

Patient	Age (y)	Sex	BMI (kg/m^2)	ICU diagnosis	APACHE-4 score	Duration of MV (h)
1	56-60	M	26	Trauma	139	33.3
2	80-85	M	25	Trauma	94	44.3
5	30-35	F	27	Trauma	76	50.5
6	30-35	M	22	Trauma	76	50.8
8	80-85	M	23	Sepsis	130	28.3
9	60-65	M	25	Trauma	94	17
10	20-25	M	24	Trauma	63	79
11	70-75	M	29	Trauma	40	5
14	70-75	M	28	Resp. failure	97	49
15	66-70	M	20	Resp. failure	104	4
C010	20-25	M	23	-	-	-
C011	20-25	M	22	-	-	-
C-09	56-60	M	26	-	-	-
C-10	50-55	F	23	-	-	-
C-11	56-60	M	32	-	-	-

Table 7. Patient characteristics in Quadriceps experiment

	Control (n=5)	ICU quadriceps (n=10)	P-value
Age (years)	42 ± 19	59 ± 23	0.148
M (%)	4 (80)	9 (90)	0.591
BMI (Kg/m^2)	25 ± 4	25 ± 3	0.864
APACHE-4	-	97 ± 31	-
Ventilation (hours)	-	36 ±23	-
Myofiber CSA (μm^2)	6509 [4828-9339]	4438 [3723-5816]	0.199

BMI = Body Mass Index APACHE = Acute Physiology And Chronic Health Evaluation, CSA = Cross-Sectional Area

Table 8. Patient characteristics in PAX-7 staining experiment

	Control (n=8)	ICU atrophy (n=8)	P-value
Age (years)	64 [58-73]	69 [60-73]	0.798
M (%)	5 (63)	5 (63)	1.0
BMI (Kg/m^2)	28 [25-30]	25 [22-29]	0.328
APACHE-3	-	72 [15-124]	-

Ventilation (hours)	1.3 [0.8-1.5]	74 [49-131]	<0.001
Myofiber CSA (μm^2)	2180 [1667-2856]	1192 [952-1709]	0.015

BMI = Body Mass Index APACHE = Acute Physiology And Chronic Health Evaluation, CSA = Cross-Sectional Area

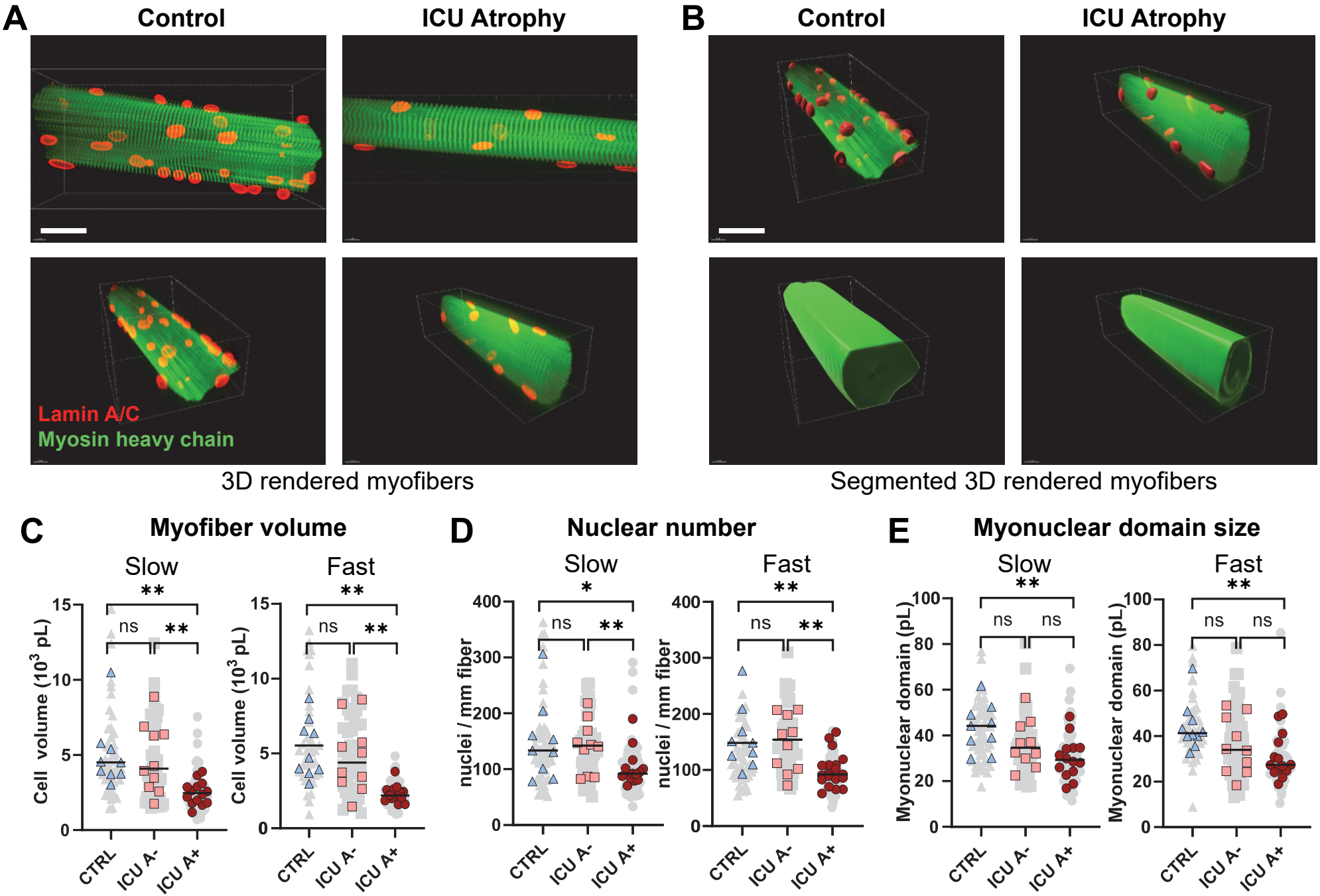
A
Control
ICU Atrophy
B
Control
ICU Atrophy
Lamin A/C
Myosin heavy chain
3D rendered myofibers
Segmented 3D rendered myofibers
C
Myofiber volume
Slow
Fast
Cell volume (10^3 pL)
D
Nuclear number
nuclei / mm fiber
E
Myonuclear domain size
Myonuclear domain (pL)
CTRL
ICU A-
ICU A+
ns
*
**

Figure 1

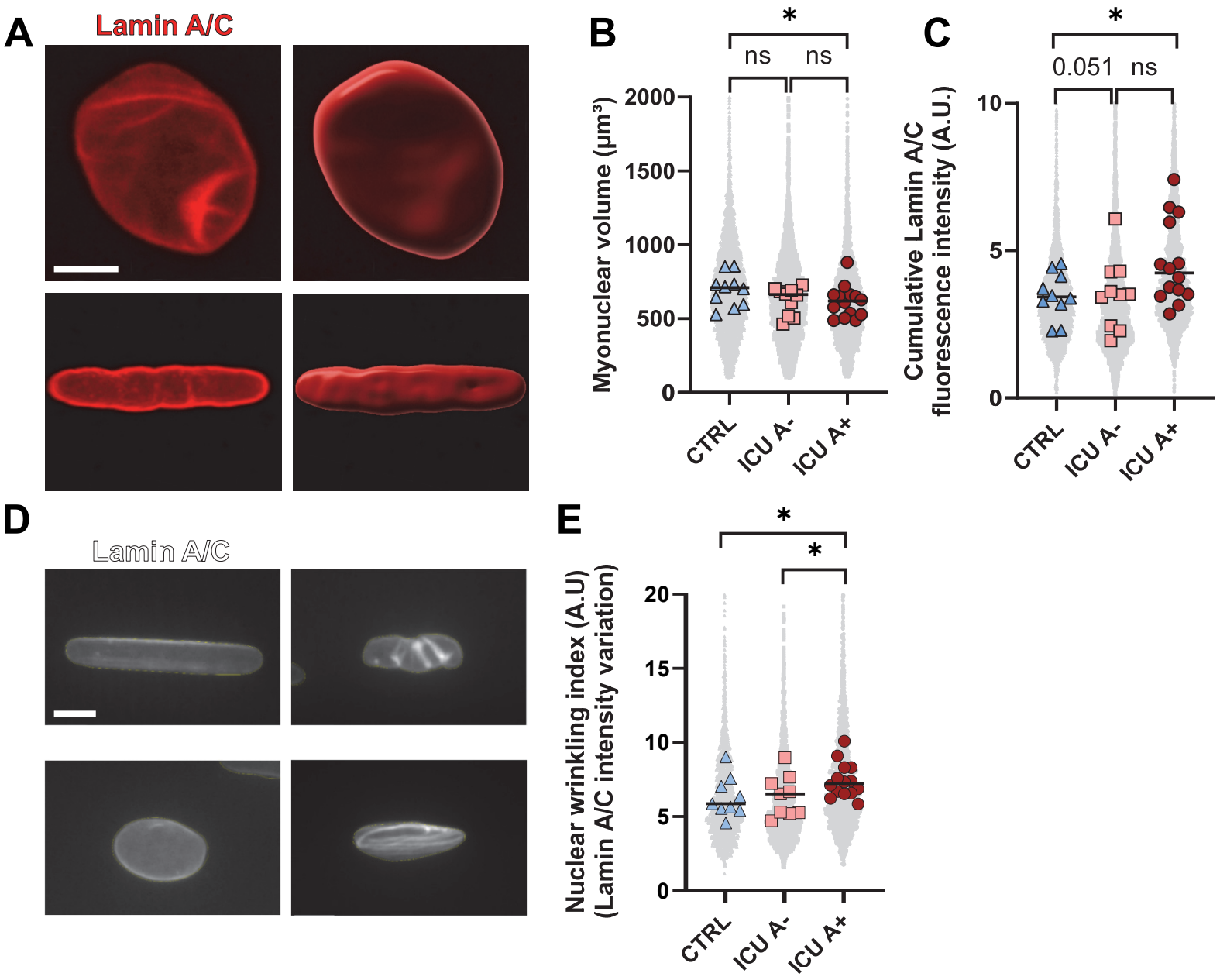
A
Lamin A/C
B
*
ns
ns
Myonuclear volume (µm³)
2000
1500
1000
500
0
CTRL
ICU A-
ICU A+
C
*
0.051
ns
Cumulative Lamin A/C fluorescence intensity (A.U.)
10
5
0
CTRL
ICU A-
ICU A+
D
Lamin A/C
E
*
*
Nuclear wrinkling index (A.U)
(Lamin A/C intensity variation)
20
15
10
5
0
CTRL
ICU A-
ICU A+

Figure 2

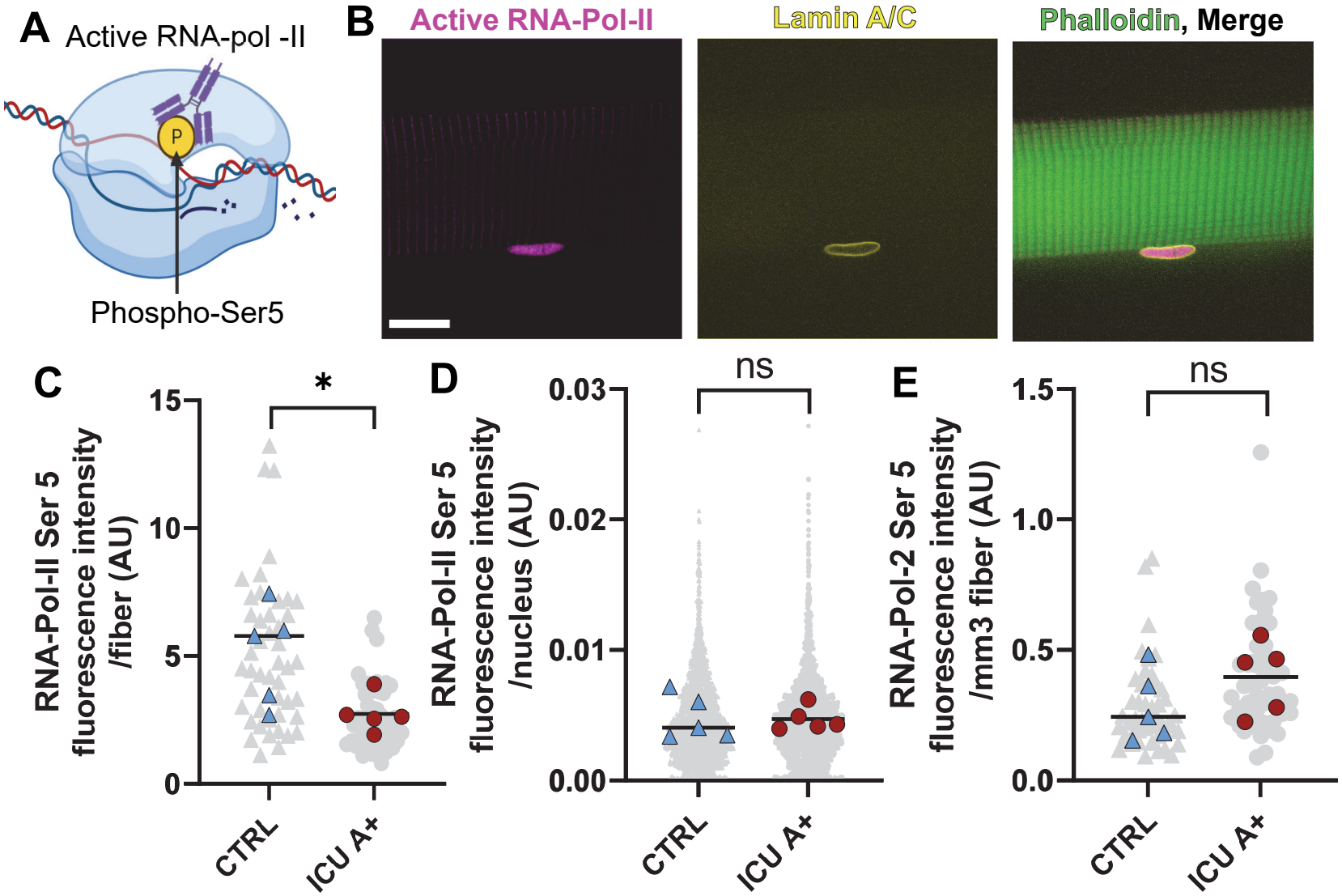
A
Active RNA-pol -II
P
Phospho-Ser5
B
Active RNA-Pol-II
Lamin A/C
Phalloidin, Merge
C
RNA-Pol-II Ser 5 fluorescence intensity /fiber (AU)
15
10
5
0
*
CTRL
ICU A+
D
RNA-Pol-II Ser 5 fluorescence intensity /nucleus (AU)
0.03
0.02
0.01
0.00
ns
CTRL
ICU A+
E
RNA-Pol-2 Ser 5 fluorescence intensity /mm3 fiber (AU)
1.5
1.0
0.5
0.0
ns
CTRL
ICU A+

Figure 3

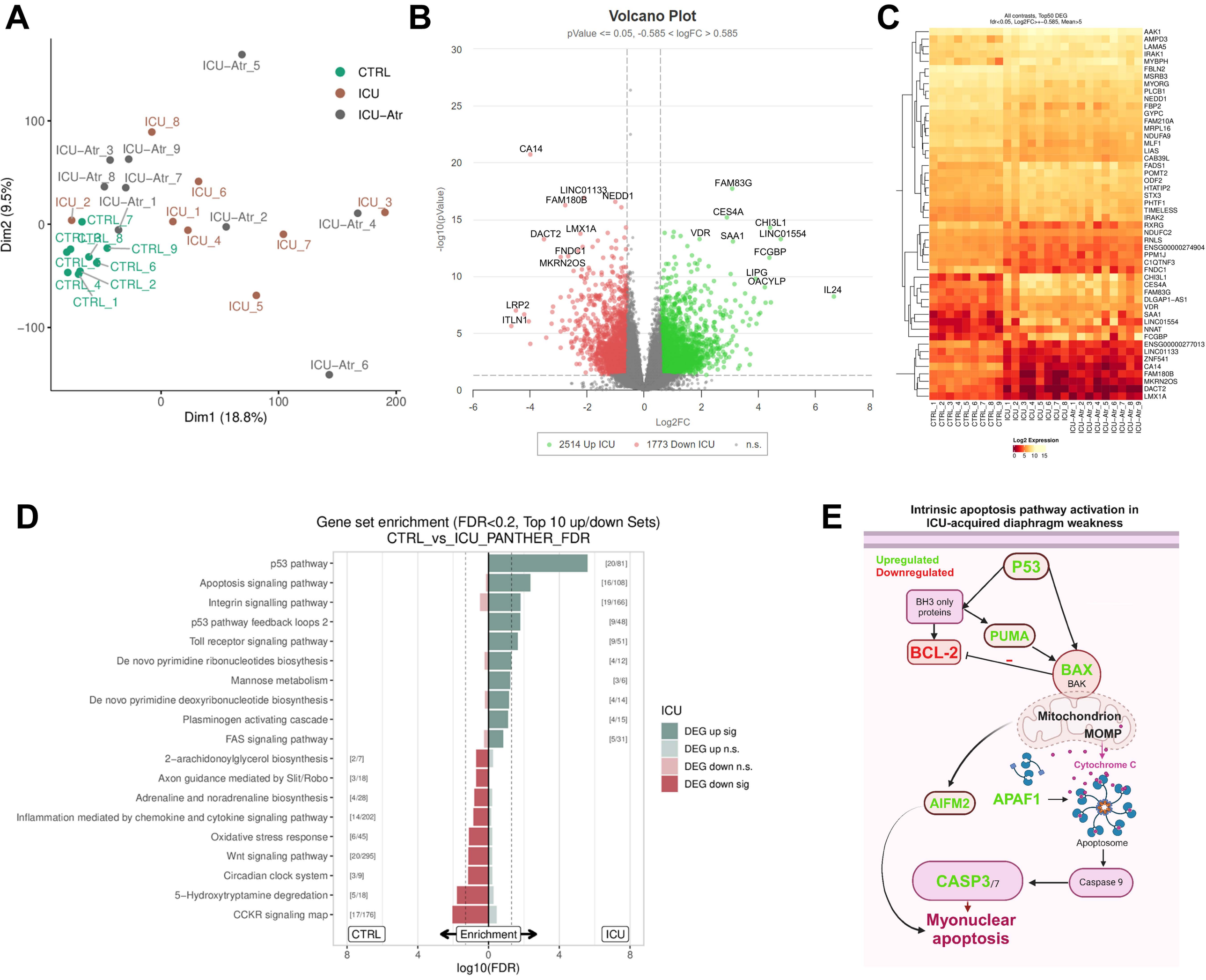
A
CTRL
ICU
ICU–Atr
Dim1 (18.8%)
Dim2 (9.5%)
B
Volcano Plot
pValue <= 0.05, -0.585 < logFC > 0.585
-log10(pValue)
Log2FC
2514 Up ICU
1773 Down ICU
n.s.
C
All contrasts, Top50 DEG
fdr<0.05, Log2FC>+-0.585, Mean>5
Log2 Expression
D
Gene set enrichment (FDR<0.2, Top 10 up/down Sets)
CTRL_vs_ICU_PANTHER_FDR
p53 pathway
Apoptosis signaling pathway
Integrin signalling pathway
p53 pathway feedback loops 2
Toll receptor signaling pathway
De novo pyrimidine ribonucleotides biosythesis
Mannose metabolism
De novo pyrimidine deoxyribonucleotide biosynthesis
Plasminogen activating cascade
FAS signaling pathway
2–arachidonoylglycerol biosynthesis
Axon guidance mediated by Slit/Robo
Adrenaline and noradrenaline biosynthesis
Inflammation mediated by chemokine and cytokine signaling pathway
Oxidative stress response
Wnt signaling pathway
Circadian clock system
5–Hydroxytryptamine degredation
CCKR signaling map
CTRL
Enrichment
ICU
log10(FDR)
DEG up sig
DEG up n.s.
DEG down n.s.
DEG down sig
E
Intrinsic apoptosis pathway activation in
ICU-acquired diaphragm weakness
Upregulated
Downregulated
P53
BH3 only proteins
PUMA
BCL-2
BAX
BAK
Mitochondrion
MOMP
Cytochrome C
AIFM2
APAF1
Apoptosome
CASP3/7
Caspase 9
Myonuclear apoptosis

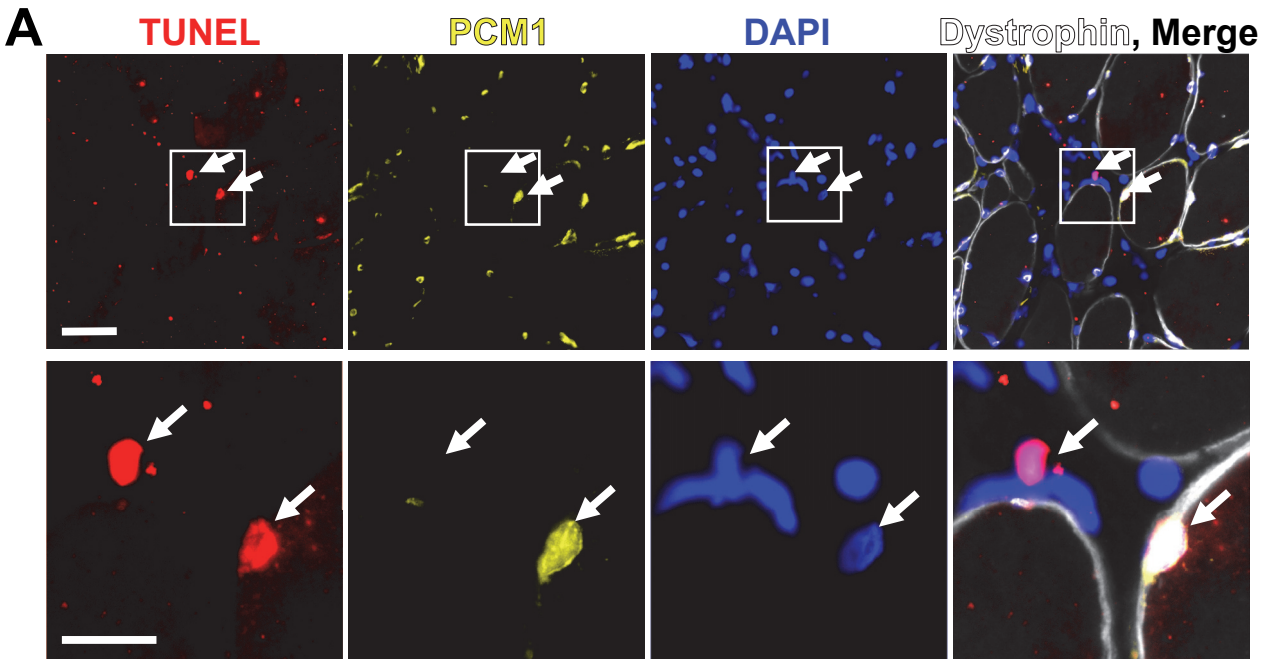
A
TUNEL
PCM1
DAPI
Dystrophin, Merge

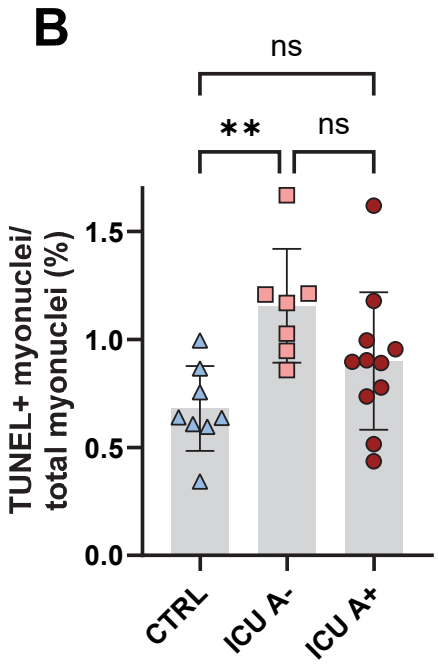
B
ns
**
ns
TUNEL+ myonuclei/
total myonuclei (%)
1.5
1.0
0.5
0.0
CTRL
ICU A-
ICU A+

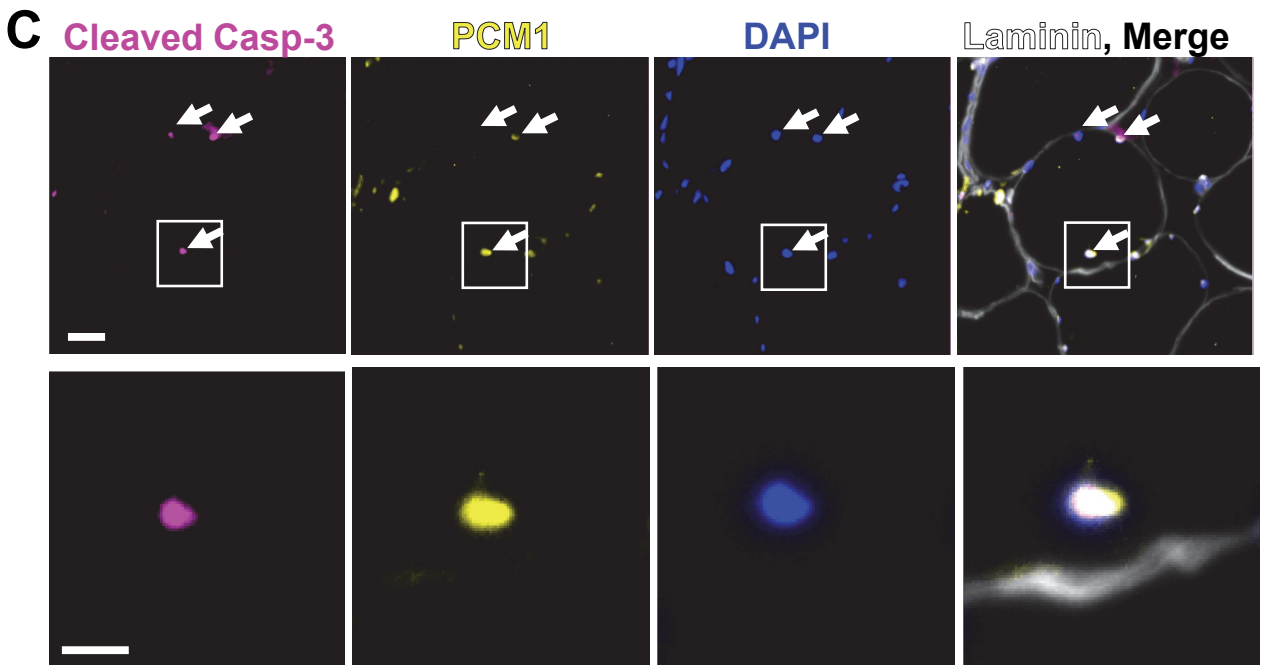
C
Cleaved Casp-3
PCM1
DAPI
Laminin, Merge

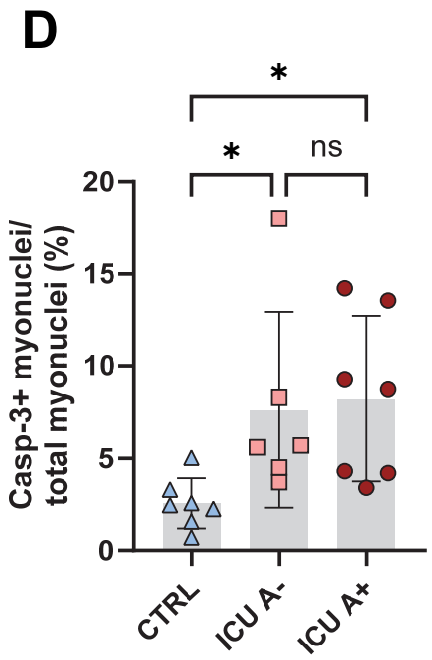
D
*
*
ns
Casp-3+ myonuclei/
total myonuclei (%)
20
15
10
5
0
CTRL
ICU A-
ICU A+

Figure 5

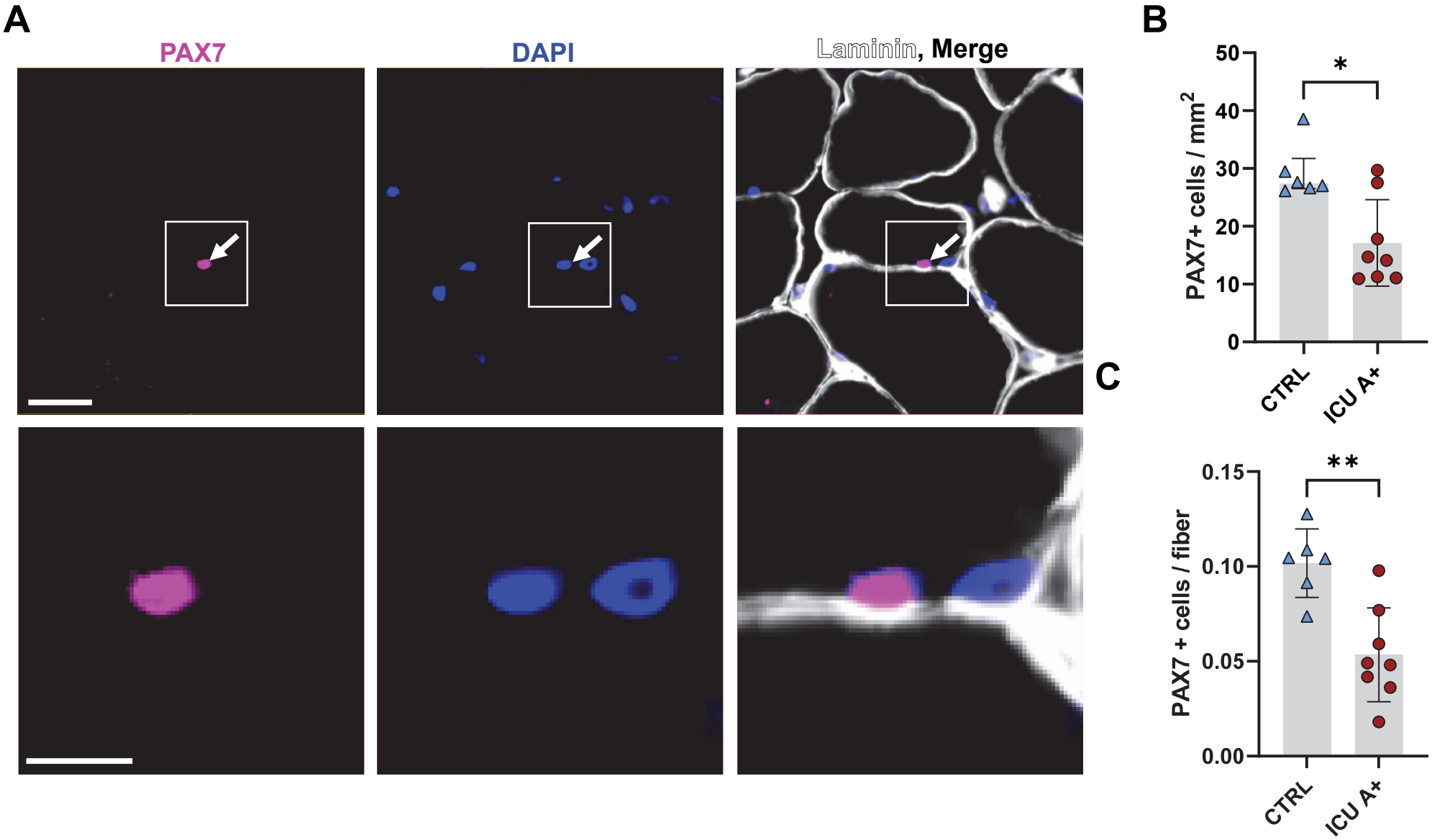
A
PAX7
DAPI
Laminin, Merge
B
PAX7+ cells / mm2
50
40
30
20
10
0
*
CTRL
ICU A+
C
PAX7 + cells / fiber
0.15
0.10
0.05
0.00
**
CTRL
ICU A+

Figure 6

Graphical summary

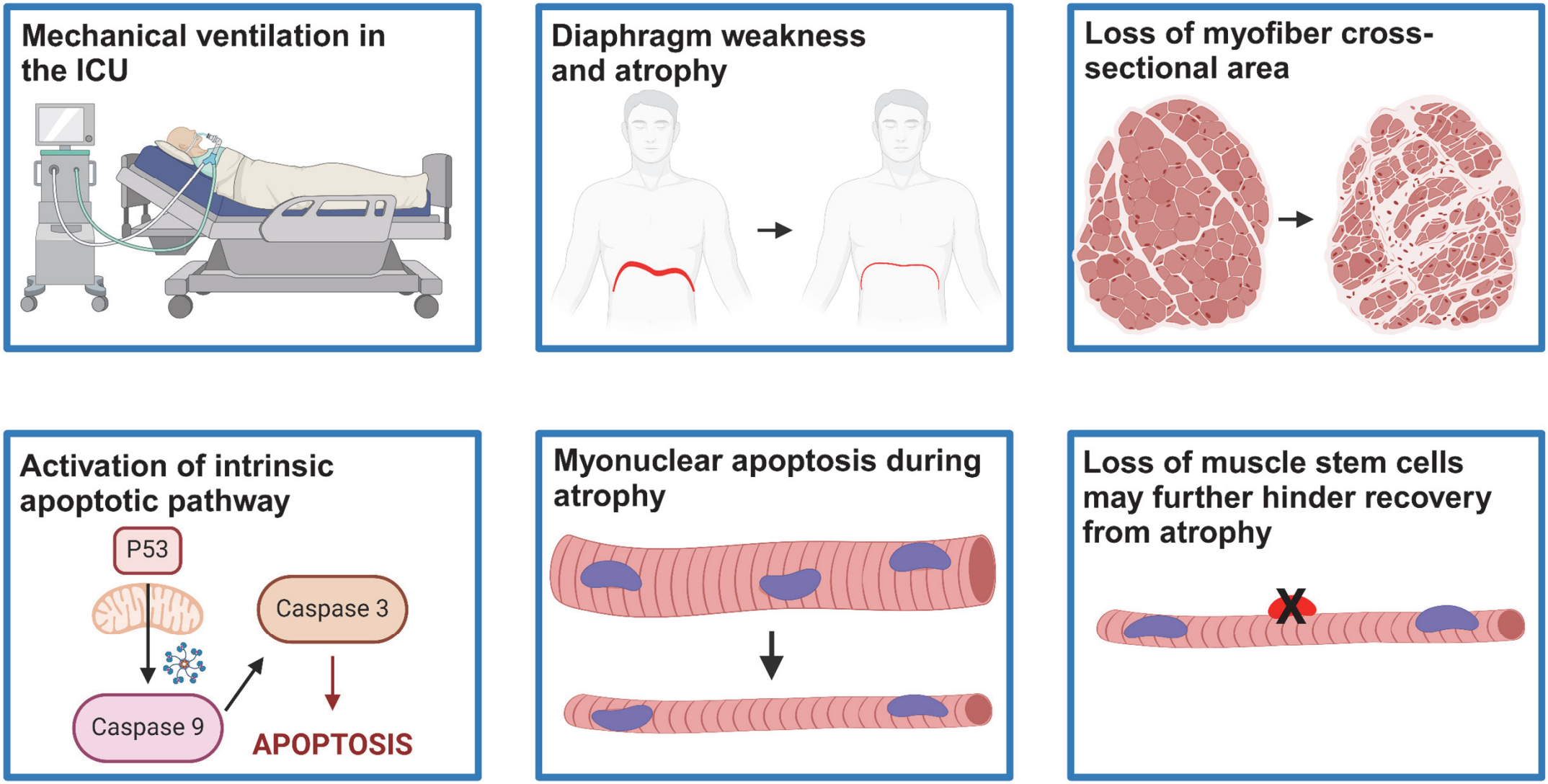

Figure 7